Extreme Mechanics Letters 2 (2015) 37–45

Contents lists available at ScienceDirect

Extreme Mechanics Letters

journal homepage: www.elsevier.com/locate/eml

Indium Tin Oxide (ITO) serpentine ribbons on soft substrates stretched beyond 100%

Shixuan Yang, Eley Ng, Nanshu Lu *

Center for Mechanics of Solids, Structures and Materials, Department of Aerospace Engineering and Engineering Mechanics, Texas Materials Institute, The University of Texas at Austin, Austin, TX 78712, USA

HIGHLIGHTS

- Simple process is developed to fabricate ITO serpentine ribbons on soft substrates.
- Weakly-bonded, long-armed serpentines can be stretched beyond 100%.
- Well-bonded, long-armed serpentines fail by transverse buckle-delamination.
- Narrower serpentines are always more stretchable if everything else fixed.

ARTICLE INFO

Article history:
Received 4 December 2014
Received in revised form 22 January 2015
Accepted 23 January 2015
Available online 25 January 2015

Keywords:
Indium Tin Oxide (ITO)
Serpentine
Stretchable

ABSTRACT

Indium Tin Oxide (ITO) has been widely used as the electrode material in touch-screen displays and solar cells attributing to its combined high electrical conductivity and optical transparency. Moving forward from wafer based electronics to flexible/stretchable electronics, brittle electronic materials like ITO are significantly hindering the deformability of the integrated systems. To minimize strains in inorganic materials when subjected to stretch, thin metallic and ceramic films can be patterned into serpentine-shaped ribbons. Although polymer-supported metallic serpentines have received extensive studies, it has been a challenging task to fabricate brittle ceramic serpentine ribbons on stretchable substrates. In this letter, we report a low cost, completely dry fabrication process to successfully integrate brittle ITO serpentine ribbons on stretchable substrates. Uniaxial tension tests are performed with *in situ* electrical resistance measurements which are used as an indicator of the mechanical integrity of the ITO ribbons. Effects of serpentine-substrate adhesion and serpentine geometry are systematically investigated. When the adhesion is weak, stretchability as high as 200% can be achieved. When the adhesion is strong, a new failure mechanism is observed. Design guidelines can be proposed for different adhesion conditions based on this study.

1. Introduction

Flexible and stretchable electronics have demonstrated tremendous potential for displays, energy, robotics, and biomedicine. Their applications include but are not limited to paper-like electronic readers [1], rollable solar cells [2], human-mimetic robotic skins [3] and bio-integrated electronics [4]. Although inorganic semiconductors (e.g., silicon, gallium arsenide (GaAs)), conductors (e.g., copper, Indium Tin Oxide (ITO)), and dielectrics (e.g., silicon oxide, silicon nitride) are well functioning in wafer-based integrated circuits, their intrinsic stiffness and even brittleness have posed serious challenges for flexible electronics. Mechanics-enabled innovative structural designs have greatly enhanced the stretchability of inorganic electronic materials. For example, silicon and gallium arsenide (GaAs)

* Correspondence to: 210 E 24th St., Austin, TX 78712, USA. Tel.: +1 512 471 4208.
E-mail address: nanshulu@utexas.edu (N. Lu).

http://dx.doi.org/10.1016/j.eml.2015.01.010
2352-4316/

nanoribbons can be transfer printed on pre-stretched elastomer substrates to develop periodic sinusoidal wrinkles or buckles when the pre-stretch is released [5–7]. The buckled nanoribbons are able to accommodate large applied tensile or compressive displacements through rigid body rotation, with minimum strains induced in the ribbons. Since electronics with out-of-plane buckles are difficult to pack or attach to other surfaces, a recently more popular stretchable structure comprises of isolated stiff islands interconnected by in-plane serpentine-shaped (i.e., meandering) thin metal ribbons. When the substrate is stretched, due to the large elastic mismatch between the islands and the soft substrate, the rigid islands stay almost undeformed while the interisland serpentine ribbons have to rotate and buckle out-of-plane to provide large extension [8–11]. A more extreme case involves freestanding, long-armed serpentine metal interconnects, which can extend more than 1000% without rupture [12]. In addition to stretchability, the other benefit of patterning stiff membranes into serpentine shapes is to achieve structural compliance [13]. For example, a filamentary serpentine network of gold with vanishing rigid islands has enabled mechanically invisible electronic tattoos to be intimately integrated with human skin for non-invasive electrophysiological, thermal, and hydration sensing [14–17], as well as wearable soft antenna for wireless communication [18]. The mechanics of metallic serpentines has also been studied extensively through both experimental [8,19–21] and theoretical/numerical means [22–26].

Except for metal-based stretchable interconnects and stretchable sensors, stretchable continuous ceramic structures have also found many applications where long length or large areal coverage is needed. For example, transfer-printed single crystalline silicon has been patterned into filamentary serpentines for stretchable epidermal amplifiers and solar cells [14]. Stretchable ceramics such as buckled lead zirconium titanate (PZT) ribbons [27] and buckled and serpentine zinc oxide (ZnO) ribbons [28] are popular materials for biomechanical energy harvesting applications attributing to their superior piezoelectric properties compared to organic piezoelectric materials [29]. However, up to now, ceramic serpentine ribbons are far less used than metal serpentines, due to their challenging fabrication processes and less understood mechanical behaviors.

While stretchable metallic serpentine ribbons can be fabricated on polymer substrates by thin film deposition and patterning through either lift-off [21,30] or etch-back [8,19] process, so far no simple method is available for the fabrication of ceramic serpentine ribbons on stretchable substrates. The only successfully demonstrated method is to transfer-print ceramic nanomembranes (either silicon or ZnO) from silicon on insulator (SOI) wafer to polymer substrates and the nanomembranes are patterned into serpentine ribbons through dry etching either before or after the transfer [14,28]. The stretchability of these brittle serpentine ribbons, however, has never been tested.

We report the first stretchability test of ceramic serpentine ribbons bonded to stretchable substrates using ITO as a model material. Thin ITO films are widely used as the electrode material in flat panel displays [31] and solar cells [32] attributing to their combined high electrical conductivity and optical transparency. However, cracks are observed at applied tensile strains around 1% in polymer-supported blanket thin ITO films [33–35]. Even ITO serpentine ribbons are found no more stretchable than their linear counterparts when supported by a stiff polymer such as Kapton [36]. Even though ITO can be sputtered and tested on Kapton, when it is sputtered on soft substrates such as polydimethylsiloxane (PDMS), ITO cannot remain intact when the soft substrate is peeled off from the sample holder. As a result, a transferring process has been developed to integrate ITO on PDMS, but the process is tedious and costly and the reported stretchability is still very limited (15%) [37].

In this paper, we report a low cost, completely dry fabrication process to successfully integrate brittle ITO serpentine ribbons on stretchable substrates. The stretchability of ITO serpentine ribbons is measured by *in situ* electromechanical experiments, and is found to depend on not only the serpentine shape but also the ribbon-substrate adhesion. When the adhesion is weak, stretchability as high as 200% can be achieved. When the adhesion is strong, a new failure mechanism is observed. Design guidelines can be proposed for different adhesion conditions based on this study. The paper is organized as follows. Section 2 describes the fabrication process and testing setup. Experimental results are provided in Section 3 and conclusions are drawn in Section 4.

2. Fabrication and testing

Since ITO is too brittle to be directly supported by soft substrates, we develop a completely dry patterning and transferring process to achieve ITO serpentine ribbons either weakly or strongly bonded on soft substrates. The whole process is illustrated by Fig. 1 schematics. Fig. 1(A) shows a piece of 13 μm thick transparent polyethylene terephthalate (PET) film (Goodfellow Corp.) pre-cleaned by acetone and isopropyl alcohol (IPA) and attached to a thermal release tape (TRT) (Semiconductor Equipment Corp.), which is supported by a cutting mat. The cutting mat is fed into an electronic cutting machine (Silhouette Cameo) which can cut the PET with serpentine-shaped seams as shown in Fig. 1(B). The cut PET on TRT is peeled off the cutting mat (Fig. 1(C)) and loaded into a magnetron sputter system (AJA International, USA) where 200 nm thick ITO is deposited from an ITO target (Kurt J. Lesker Company) on the PET with base pressure of 1.0×10^{-7} torr, working gas (argon) pressure of 2.0×10^{-3} torr, and RF power of 60 W (Fig. 1(D)). After deposition, the ITO covered PET is transferred to another TRT as shown in Fig. 1(E). To achieve well-bonded serpentines, 5 nm Ti and 50 nm SiO_2 are sputtered on the backside of PET, i.e., the surface not covered by ITO, as shown in Fig. 1(F). When the TRT is heated to 115 °C on a hot plate, the excessive PET can be easily peeled off with the pre-formed seams, leaving only serpentine ribbons on the TRT (Fig. 1(G)). The serpentine ribbons can be transfer-printed onto Tegaderm (3M), a transparent wound dressing polymer tape with thickness of 47 μm and Young's modulus of 7.43 MPa, whose adhesive surface is treated by ultraviolet ozone (UVO) for 5 min (Fig. 1(H)), rendering the final sample as shown in Fig. 1(I). UVO treated polymer

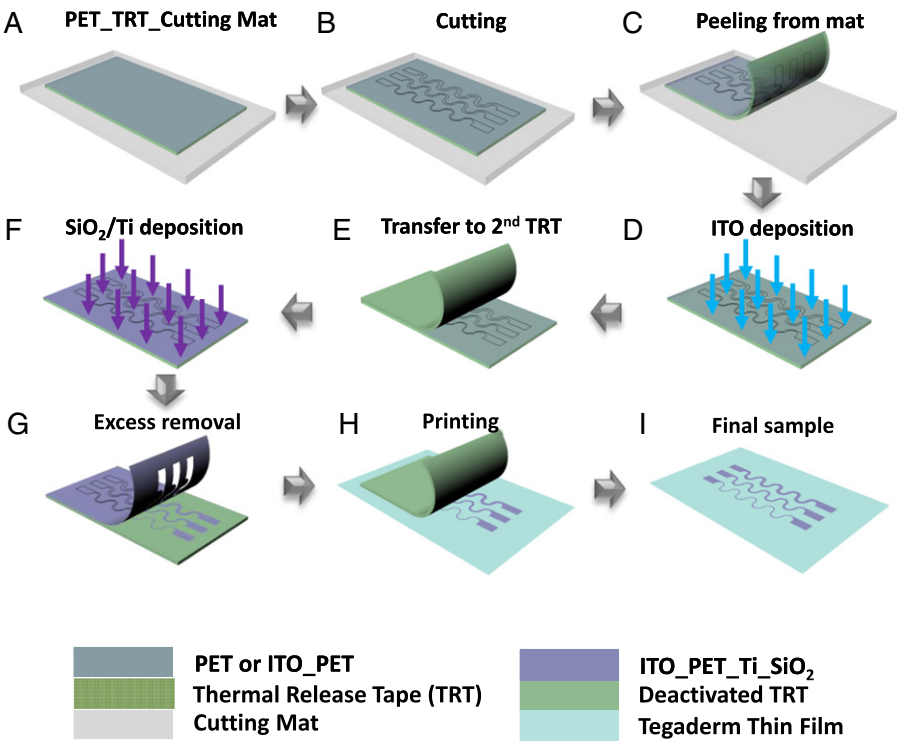

Fig. 1. Schematics of the dry, bench top fabrication process of stretchable ITO serpentines on stretchable Tegaderm substrates: A, laminating 13 μm thick PET on TRT on cutting mat. B, using an electronic cutter to carve serpentine-shaped seams on PET. C, peeling TRT-supported PET from the cutting mat. D, sputtering 200 nm thick ITO on PET. E, transferring ITO covered PET from one TRT to another with the backside of PET exposed. F, sputtering 5 nm Ti and 50 nm SiO_2 on the backside of the PET (for weakly-bonded serpentines, this step is skipped). G, removing unwanted PET, leaving only ITO_PET serpentines on the TRT. H, printing the ITO_PET serpentine ribbons on Tegaderm. I, the final sample.

can form hydrophilic surface which is able to form strong chemical bonding through condensation reactions with the SiO_2 layer deposited on the backside of the PET. In addition to Tegaderm, other stretchable substrates such as PDMS and Ecoflex can also be used through the same bonding process. For weakly-bonded samples, SiO_2 deposition (Step F) and UVO treatment of Tegaderm are omitted, but the native adhesive on Tegaderm can still ensure successful transfer of the serpentine ribbons. The whole process takes less than 15 min excluding the deposition time and the yield is almost 100%.

The Tegaderm-supported ITO samples are shown in Fig. 2. Unlike some other serpentine interconnects which are sandwiched by stiff polymer layers [8,9,14], the surfaces of our ITO serpentines are exposed for easier electrical measurement. To study the effect of serpentine geometry on its stretchability, four geometric parameters are defined in Fig. 2(A) following the convention used in our previous two serpentine studies [13,36]: the ribbon width w, the arc radius r, the arc angle α, and the arm length l, which can yield three dimensionless geometric parameters w/r, l/r and α. Fig. 2(B) shows three groups of as-fabricated, well-bonded ITO/PET serpentines on Tegaderm, which will be used to study the width effect, the arm length effect, and the arc angle effect. The terminal pads are designed for easier electrical contacts and they will be fully clamped by the grips of the stretcher when tension tests are performed. The gray color of the ribbons comes from the Ti layer. For weakly-bonded serpentines without the Ti layer, the transparency of ITO is evidenced by Fig. 2(C).

Since ITO is mechanically brittle and electrically conductive, resistance vs. applied strain curves have been widely adopted to indicate the overall mechanical integrity of thin ITO films as a function of strain [34–36]. The resistance vs. applied strain curve can be tested by an *in situ* electromechanical setup as shown in Fig. 3(A). For each uniaxial tension test, a Tegaderm substrate supporting a group of 2 or 3 serpentine ribbons is gripped on a home-made manual stretcher. The applied strain, ε_{app}, is calculated as the ratio of the applied displacement to the initial gauge length. The ITO ribbons are connected through an anisotropic conductive film (ACF, Elform) to a multi-channel data acquisition (DAQ) system (NI USB-6225) which is configured to conduct resistance measurements up to 3 channels. The electrical resistance of as-fabricated ITO serpentines are of the order of $10^5\,\Omega$, which is high compared to some other ITO thin films [38,39] and is attributed to our non-optimized ITO sputtering recipe. The dry transfer printing process does not crack the ITO serpentine because the ITO resistance remains the same before and after transfer printing. The behavior of ITO serpentines during stretch is continuously observed by a top-down webcam. Two typical normalized resistance vs. strain curves are offered in Fig. 3(B). It has been well proved that the explosion of the curve is closely correlated with the mechanical failure of the ITO film [34–36]. The quantitative definition of stretchability is somewhat arbitrary

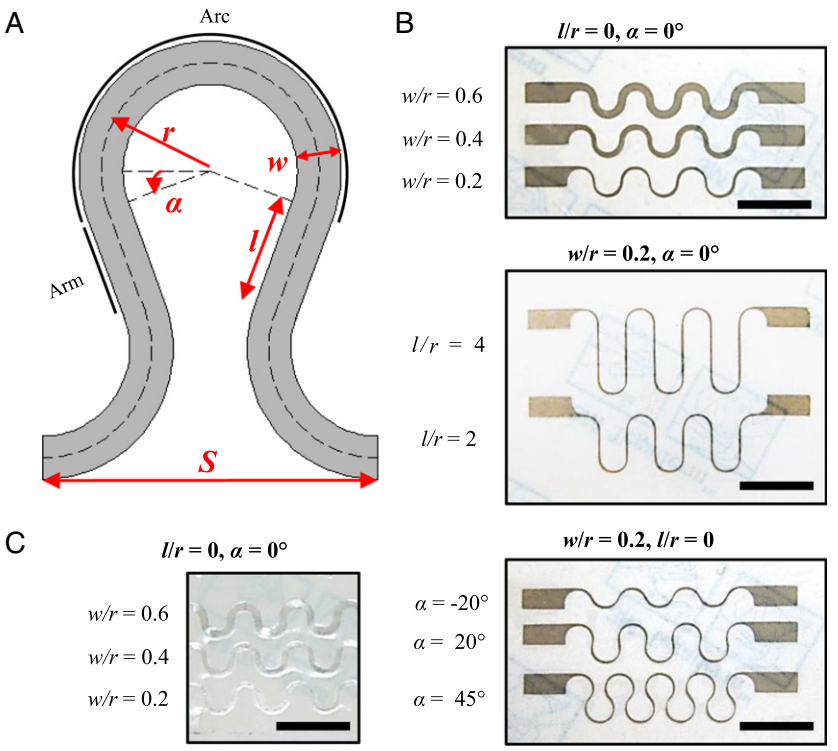

Fig. 2. A, definition of the geometric parameters of a serpentine: ribbon width w, arm length l, arc radius r, arc angle α, and horizontal span S. B, pictures of three groups of well-bonded ITO serpentines with systematically varied geometries. C, a picture of a weakly-bonded ITO displays good transparency. The scale bar is 5 mm in all pictures.

and in this paper, we define *stretchability*, i.e., the critical strain-to-rupture, ε_{app}^{cr}, as the tensile strain applied to the substrate at which $R/R_0 = 6$. A representative resistance vs. strain curve for straight serpentine ribbon is given in Fig. 3(B), with a blown up view included as the inset. The stretchability of a straight ITO ribbon is found to be between 0.77% and 1.5%, with an average of 1.12%, which is in good agreement with previous stretchability tests on blanket ITO films [34,35] or straight ITO ribbons [36], indicating that stretchability obtained by our electromechanical measurement is reliable. For the serpentine specimen shown in Fig. 3(B) whose shape is given by $w/r = 0.2$, $l/r = 2$, $\alpha = 0^\circ$ and adhesion to Tegaderm is weak, the stretchability is found to be 113%, which represents a 100 fold enhancement over the straight ITO stretchability. It is the first time that a continuous ITO ribbon can be stretched beyond 100%.

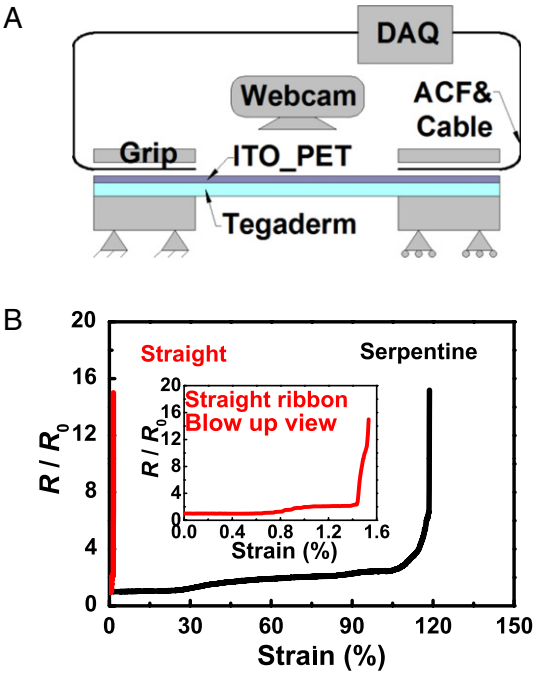

Fig. 3. A, the electromechanical setup with *in situ* top view. B, resistance vs. strain curves of a straight and a serpentine ribbon. If $R/R_0 = 6$ is used as the cutoff criterion, then the stretchability is 1.46% for the straight ribbon and 113% for the serpentine ribbon.

3. Results

3.1. Weakly-bonded serpentine ribbons

The effects of serpentine shape and serpentine-to-substrate adhesion have been systematically investigated. Fig. 4 summarizes the results of weakly-bonded serpentines, which can easily detach from Tegaderm or in another word, the strain-to-debond is small. First, the effect of ribbon width is revealed in Fig. 4(A) & (B), using the ribbon shapes given in the top panel of Fig. 2(B), whose $\alpha = 0^\circ$,

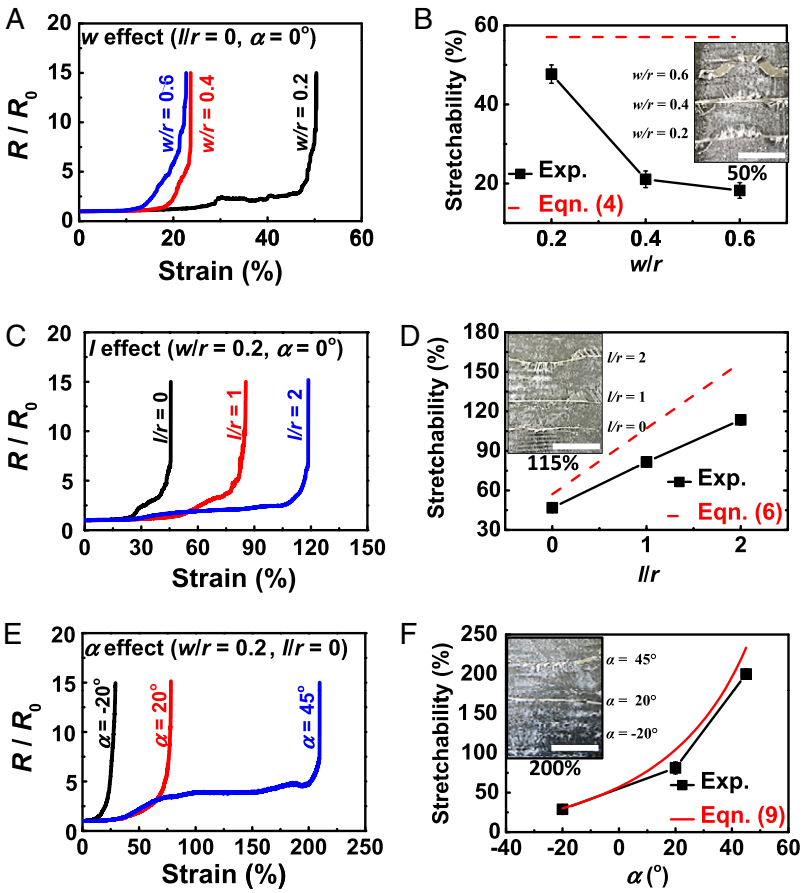

Fig. 4. Resistance vs. strain plots and stretchability plots for weakly-bonded serpentines. A&B, serpentines with different ribbon widths (w effect); C&D, serpentines with different arm lengths (l effect); and E&F, serpentines with different arc angles (α effect). The scale bar is 2 mm in all insets. (For interpretation of the references to color in this figure legend, the reader is referred to the web version of this article.)

$l/r = 0$, but $w/r = 0.6$, 0.4, and 0.2, respectively. The resistance vs. strain curves for those three serpentines are given in Fig. 4(A) and the corresponding stretchability vs. w/r plot is given in Fig. 4(B). Error bars in all the stretchability figures come from at least three measurements. It is clear that with everything else the same, the narrower serpentine ribbons are more stretchable, which is consistent with the trend observed for freestanding serpentines [13] as well as Kapton-supported ITO serpentines [36]. The inset in Fig. 4(B) shows a top view of the specimen at an applied strain of 50%, which is right after the most stretchable serpentine, i.e., the one with $w/r = 0.2$, ruptures. It is evidenced by the inset that the $w/r = 0.2$ serpentine is almost fully debonded and straightened when it ruptures. The delamination is most severe at the arcs, which is consistent with other experimental observations of serpentine delamination [19,40]. Peak strain will always occur near the crest of the arc according to numerous finite element modeling (FEM) results of freestanding or popped-up serpentines [8,13,22], hence the debonded serpentine fails by crest rupture. For the two wider serpentines, however, our *in situ* top down observation during the electromechanical tests indicates that they rupture before delamination, which results in much lower stretchability. Cracks are also expected to first appear near the crest based on the FEM results of substrate-bonded serpentines [23,36,41]. If we differentiate the strain-to-rupture before delamination and after delamination to be bonded and debonded strain-to-rupture, it can be concluded that for narrow serpentines, strain-to-debond is smaller than bonded strain-to-rupture but wide ribbons exhibit smaller bonded strain-to-rupture than strain-to-debond.

If we assume delaminated serpentines becomes freestanding and eventually rupture when they are fully straightened, then their ultimate stretchability is limited by the total curve length of the serpentine, i.e.,

$$\varepsilon_{\text{app}}^{\text{cr}} = \frac{c - S}{S}, \tag{1}$$

where S is the horizontal span of a unit cell as labeled in Fig. 2(A) and c represents the curve length of a unit cell. For ribbons with $\alpha = 0^\circ$ and $l/r = 0$,

$$S = 4r, \tag{2}$$

and

$$c = 2\pi r. \tag{3}$$

Plugging Eqs. (2) and (3) into Eq. (1) yields a constant debonded strain-to-rupture

$$\varepsilon_{\text{app}}^{\text{cr}} = \frac{\pi - 2}{2}, \tag{4}$$

which is plot as a red horizontal line in Fig. 4(B). The stretchability of $w/r = 0.2$ serpentine is found slightly smaller than the predicted ideal stretchability due to stresses induced by unwinding and residual constraints from the adhesives. It can be expected that the narrower serpentines will better approach the ultimate stretchability limit. The stretchability of wider serpentines appear to be much lower than the horizontal line because they rupture before debond.

The effect of arm length is studied in Fig. 4(C) & (D), using ribbons with $w/r = 0.2$, $\alpha = 0^\circ$, and $l/r = 0$, 1, and 2, respectively. Fig. 4(D) indicates a linear increase of stretchability with arm length. Our *in situ* observation confirms that all three ribbons detach before rupture, as represented by the inset of Fig. 4(D). To predict the ultimate stretchability of serpentines with $\alpha = 0^\circ$ and different l, their S is captured by Eq. (2) and c is given by

$$c = 2\pi r + 2l. \tag{5}$$

Plugging Eqs. (2) and (5) into Eq. (1) yields

$$\varepsilon_{\text{app}}^{\text{cr}} = \frac{\pi - 2 + \frac{l}{r}}{2}, \tag{6}$$

which is a linear function of l/r, as plotted in Fig. 4(D). The growing difference between measured stretchability and Eq. (6) as l enlarges suggests increasing constraints from the adhesive on serpentines with large transverse dimensions.

The effect of arc angle is given in Fig. 4(E) & (F), using ribbons displayed in the bottom panel of Fig. 2(B), whose $w/r = 0.2$, $l/r = 0$, and $\alpha = -20^\circ$, 20°, and 45°, respectively. The stretchability of $\alpha = 45^\circ$ ribbon has reached 200%, which is an exciting achievement considering how brittle ITO is. Delamination is clearly seen in the inset of Fig. 4(F) when the substrate is stretched by 200%. In fact, the $\alpha = -20^\circ$ ribbon is missing in the inset due to too much slippage. The horizontal span of ribbons with $l/r = 0$ and varying α is given by

$$S = 4r\cos(\alpha), \tag{7}$$

and the total curve length of the α-effect ribbons can be given by

$$c = 2(\pi + 2\alpha)r. \tag{8}$$

Plugging Eqs. (7) and (8) into Eq. (1) will yield the prediction of the ultimate stretchability of α-effect ribbons,

$$\varepsilon_{\text{app}}^{\text{cr}} = \frac{\pi + 2\alpha - 2\cos(\alpha)}{2\cos(\alpha)}, \tag{9}$$

which is plotted as a red curve in Fig. 4(F). The close agreement between the measured and predicted stretchability indicates that rupture happens when the ribbons are almost fully straightened. Like the l-effect ribbons, the growing discrepancy for serpentines with larger transverse dimensions is also found in α-effect ribbons.

In summary, Fig. 4 studies the stretchability of various ITO serpentines weakly-bonded to stretchable Tegaderm substrate. Although our *in situ* setup of webcam cannot offer close-up crack visualization, through combined resistance measurement and macroscopic morphology observation, four important conclusions can be reached: (1) delamination initiate from the arcs of the serpentine and merge in the middle; (2) wide serpentine ribbons tend to rupture before delamination while narrow serpentines delaminate before rupture; (3) the stretchability of serpentines with narrow width and small transverse dimension can approach the predicted ultimate stretchability; and (4) according to the predicted stretchability, a very simple way to enhance the stretchability of weakly-bonded serpentine is to use narrow serpentine ribbons with long arm or large α. These conclusions are drawn for weakly bonded serpentine ribbons, whereas the behaviors of well-bonded serpentine ribbons will be very different.

3.2. Well-bonded serpentine ribbons

Fig. 5 investigates the stretchability of well-bonded ITO serpentines on Tegaderm. For this type of specimens the detachment from substrate is retarded but it does not mean that delamination is fully prohibited. Overall the stretchability is lower compared with weakly bonded ones because of the stronger substrate constraint. Following the same order as Figs. 4, 5(A) & (B) examines the ribbon width effect. The stretchability of well-bonded serpentines (plotted as black squares) is compared with that of weakly-bonded ones of the same shapes (plotted as red dots). The similarity of the two sets of data indicates that there is no significant change of failure mechanism, i.e. the $w/r = 0.2$ serpentine ruptures after delamination whereas the two wider ones rupture before delamination.

Interesting deviation appears when ribbons have different arm lengths as shown in Fig. 5(C) & (D). The insets in Fig. 5(D) offer the top view of the serpentines captured at their respective strain-to-rupture. It is found that well-bonded serpentine ribbons with $l/r = 0$, and 1 share similar stretchability with weakly-bonded counterparts, which can be explained by the two insets showing that the two ribbons have debonded before rupture. However, the stretchability of well-bonded serpentines starts to decrease when l/r increases beyond 1. A close look at well-bonded, long-armed serpentines at failure always reveals one or multiple transverse buckles within the arm as highlighted by the red circles. Such buckles are induced by the transverse contraction of the soft substrate when it is stretched longitudinally, i.e., the Poisson's effect, which is a widely observed instability phenomenon for stiff membranes bonded to soft substrates [6,7,42–48]. While carefully controlled buckling has been harnessed to achieve stretchable electronics [6,7], buckled brittle thin films are susceptible to fracture due to the local tensile strain at the buckled peaks or ridges [49,50]. Even without high enough resolution to detect where cracks first initiate, we can still infer that buckle delamination is the failure mechanism of long-armed serpentine because: first, we have found close correlation between buckling and explosion of resistance during our electromechanical experiments with *in situ* top morphology observation; second, as buckle delamination induced rupture is a sudden event of instability, their resistance vs. strain curves exhibit a steeper rise compared to serpentines rupturing at the crest of the arc; third, if there were no buckle delamination, the effect of arm length for soft-substrate-bonded serpentines should

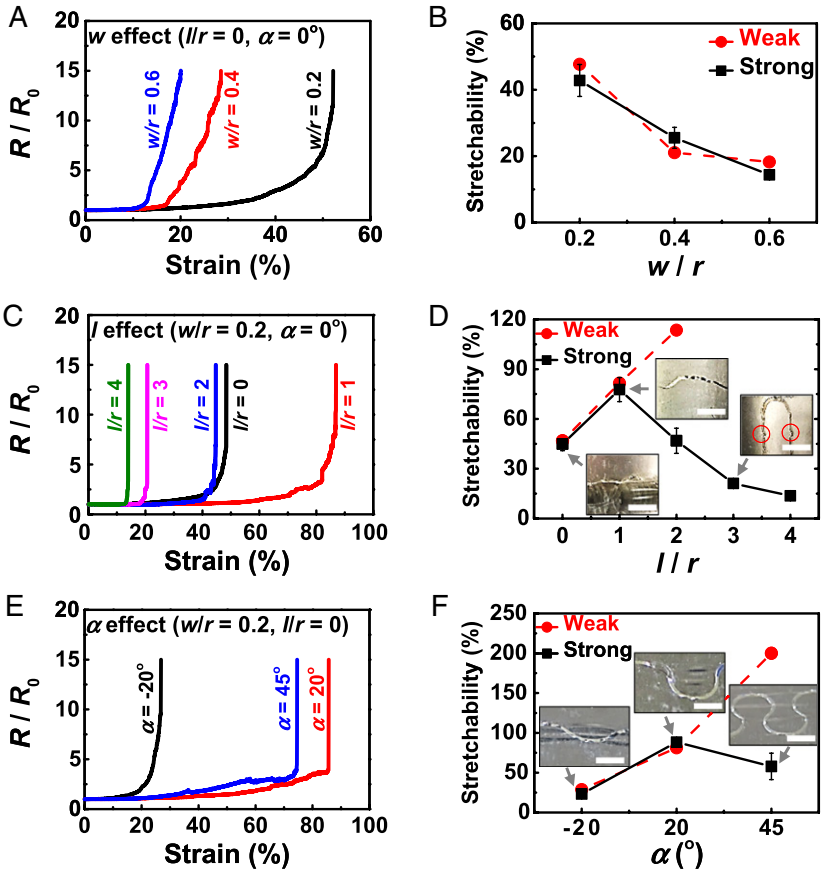

Fig. 5. Resistance vs. strain plots and stretchability plots for well-bonded serpentines. A&B, serpentines with different ribbon widths (w effect); C&D, serpentines with different arm lengths (l effect); and E&F, serpentines with different arc angles (α effect). The scale bar is 2 mm in all insets. (For interpretation of the references to color in this figure legend, the reader is referred to the web version of this article.)

be bonded by that of freestanding serpentines (the longer the arm, the more stretchable) [13] and stiff-substrate-supported serpentines (negligible arm length effect) [36], which is inconsistent with our experimental observation that the longer the arm, the less stretchable the serpentine is. Therefore we conclude that transverse buckling is a new failure mechanism of well-bonded, long-armed serpentines.

The effect of arc angle is studied in Fig. 5(E) & (F). The insets in Fig. 5(F) are also taken at their respective strain-to-rupture. When rupture happens, we can see that serpentines with $\alpha = -20^\circ$ and 20° have experienced partial delamination, which is not the case for the serpentine with $\alpha = 45^\circ$. This can explain the non-monotonic stretchability of well-bonded serpentines with respect to α. As we have mentioned before, well-bonded serpentines can still delaminate from the substrate under high enough applied strain. When there is delamination before rupture, e.g., when $\alpha = -20^\circ$ and 20°, we expect the serpentine with longer curve length to be more stretchable, hence the stretchability increases with α according to Eq. (8), and the stretchability of well-bonded serpentines are comparable with that of weakly-bonded serpentines. The effect of adhesion becomes significant when $\alpha = 45^\circ$. For weakly-bonded serpentine as shown in Fig. 4(F), the strain-to-debond is smaller than the bonded strain-to-rupture, hence after delamination, the stretchability is only limited by the unwound length of the serpentine. It is the opposite for well-bonded serpentine as shown in Fig. 5(F), where the strain-to-debond is extended due to the enhanced adhesion. As a result, the bonded strain-to-rupture is reached first and the stretchability is limited to the strain-to-rupture of fully bonded serpentines, which is small due to the tension in ITO induced by the substrate.

In summary, as substrate constraint becomes more significant, the stretchability of well-bonded serpentines is no longer always monotonic. While simply increasing the arm length or arc angle can enhance the stretchability of weakly-bonded serpentines, it is no longer true for well-bonded serpentines for two reasons. First, when the arm is too long, transverse buckling within the arms can induce rupture in ITO and the longer the arm, the earlier the rupture. The optimum arm length is found to be $l/r = 1$. Second, when α is too large, strain-to-rupture is reached before strain-to-debond. The optimum arc angle is found to be $\alpha = 20^\circ$.

4. Conclusions

We have introduced a low cost, high throughput, bench top, dry process to fabricate extremely stretchable ITO

serpentine ribbons on soft, stretchable substrates. The electromechanical measurements with *in situ* top morphology observation can reveal not only the stretchability but also the failure mechanism of these serpentines. Weakly-bonded ITO serpentine ribbons show good transparency, and are always more stretchable with narrower ribbon width, longer arms, larger arc radius, and larger arc angle. While wide serpentines rupture before debond, narrow serpentines always debond before rupture, whose ultimate stretchability can be captured by their unwound length, i.e., total curve length. The stretchability of well-bonded ribbons, however, show non-monotonic dependence on those geometric parameters due to stronger substrate constraints. It is found that serpentines with long arms rupture by transverse buckling, which degrades stretchability when the transverse dimension is large. We have limited our current investigation on one time, uniaxial tension behavior and the reversibility and cyclic behaviors of those brittle ITO serpentines require future studies.

Acknowledgments

This work is supported by the NSF CMMI award under Grant No. 1351875 and the NSF EEC NASCENT (Nanomanufacturing Systems for Mobile Computing and Mobile Energy Technologies) Center under Grant No. 1160494. N.L. acknowledges the 3M Non-Tenured Faculty Award. Eley Ng acknowledges the Undergraduate Research Fellowship (URF) from University of Texas at Austin.

References

[1] J.A. Rogers, Z. Bao, K. Baldwin, A. Dodabalapur, B. Crone, V.R. Raju, et al., Paper-like electronic displays: large-area rubber-stamped plastic sheets of electronics and microencapsulated electrophoretic inks, Proc. Natl. Acad. Sci. USA 98 (2001) 4835–4840.

[2] J. Yoon, A.J. Baca, S.I. Park, P. Elvikis, J.B. Geddes, L.F. Li, et al., Ultrathin silicon solar microcells for semitransparent, mechanically flexible and microconcentrator module designs, Nature Mater. 7 (2008) 907–915.

[3] T. Sekitani, T. Someya, Stretchable organic integrated circuits for large-area electronic skin surfaces, MRS Bull. 37 (2012) 236–245.

[4] D.H. Kim, R. Ghaffari, N.S. Lu, J.A. Rogers, Flexible and stretchable electronics for bio-integrated devices, Annu. Rev. Biomed. Eng. 14 (2012) 113–128.

[5] D.Y. Khang, H.Q. Jiang, Y. Huang, J.A. Rogers, A stretchable form of single-crystal silicon for high-performance electronics on rubber substrates, Science 311 (2006) 208–212.

[6] Y.G. Sun, W.M. Choi, H.Q. Jiang, Y.G.Y. Huang, J.A. Rogers, Controlled buckling of semiconductor nanoribbons for stretchable electronics, Nature Nanotechnol. 1 (2006) 201–207.

[7] D.Y. Khang, J.A. Rogers, H.H. Lee, Mechanical buckling: mechanics, metrology, and stretchable electronics, Adv. Funct. Mater. 19 (2009) 1526–1536.

[8] D.H. Kim, J.Z. Song, W.M. Choi, H.S. Kim, R.H. Kim, Z.J. Liu, et al., Materials and noncoplanar mesh designs for integrated circuits with linear elastic responses to extreme mechanical deformations, Proc. Natl. Acad. Sci. USA 105 (2008) 18675–18680.

[9] D.H. Kim, N.S. Lu, R. Ghaffari, Y.S. Kim, S.P. Lee, L.Z. Xu, et al., Materials for multifunctional balloon catheters with capabilities in cardiac electrophysiological mapping and ablation therapy, Nature Mater. 10 (2011) 316–323.

[10] R.H. Kim, M.H. Bae, D.G. Kim, H.Y. Cheng, B.H. Kim, D.H. Kim, et al., Stretchable, transparent graphene interconnects for arrays of microscale inorganic light emitting diodes on rubber substrates, Nano Lett. 11 (2011) 3881–3886.

[11] S. Xu, Y.H. Zhang, J. Cho, J. Lee, X. Huang, L. Jia, et al., Stretchable batteries with self-similar serpentine interconnects and integrated wireless recharging systems, Nature Commun. 4 (2013).

[12] G. Lanzara, N. Salowitz, Z.Q. Guo, F.K. Chang, A spider-web-like highly expandable sensor network for multifunctional materials, Adv. Mater. 22 (2010) 4643–4648.

[13] T. Widlund, S. Yang, Y.-Y. Hsu, N. Lu, Stretchability and compliance of freestanding serpentine-shaped ribbons, Internat. J. Solids Structures 51 (2014) 4026–4037.

[14] D.H. Kim, N.S. Lu, R. Ma, Y.S. Kim, R.H. Kim, S.D. Wang, et al., Epidermal electronics, Science 333 (2011) 838–843.

[15] X. Huang, W.H. Yeo, Y.H. Liu, J.A. Rogers, Epidermal differential impedance sensor for conformal skin hydration monitoring, Biointerphases 7 (2012) 1–9.

[16] R.C. Webb, A.P. Bonifas, A. Behnaz, Y. Zhang, K.J. Yu, H. Cheng, et al., Ultrathin conformal devices for precise and continuous thermal characterization of human skin, Nature Mater. 12 (2013) 938–944.

[17] W.-H. Yeo, Y.-S. Kim, J. Lee, A. Ameen, L. Shi, M. Li, et al., Multi-functional electronics: multifunctional epidermal electronics printed directly onto the skin (Adv. Mater. 20/2013), Adv. Mater. 25 (2013) 2772–2772.

[18] J. Kim, A. Banks, H. Cheng, Z. Xie, S. Xu, K.-I. Jang, et al., Epidermal electronics with advanced capabilities in near-field communication, Small (2014). http://dx.doi.org/10.1002/smll.201402495.

[19] Y.Y. Hsu, M. Gonzalez, F. Bossuyt, F. Axisa, J. Vanfleteren, I. De Wolf, In situ observations on deformation behavior and stretching-induced failure of fine pitch stretchable interconnect, J. Mater. Res. 24 (2009) 3573–3582.

[20] Y.Y. Hsu, M. Gonzalez, F. Bossuyt, J. Vanfleteren, I. De Wolf, Polyimide-enhanced stretchable interconnects: design, fabrication, and characterization, IEEE Trans. Electron Devices 58 (2011) 2680–2688.

[21] D.S. Gray, J. Tien, C.S. Chen, High-conductivity elastomeric electronics, Adv. Mater. 16 (2004) 393.

[22] T. Li, Z.G. Suo, S.P. Lacour, S. Wagner, Compliant thin film patterns of stiff materials as platforms for stretchable electronics, J. Mater. Res. 20 (2005) 3274–3277.

[23] M. Gonzalez, F. Axisa, F. Bossuyt, Y.Y. Hsu, B. Vandevelde, J. Vanfleteren, Design and performance of metal conductors for stretchable electronic circuits, Circuit World 35 (2009) 22–29.

[24] Y. Zhang, H. Fu, Y. Su, S. Xu, H. Cheng, J.A. Fan, et al., Mechanics of ultra-stretchable self-similar serpentine interconnects, Acta Mater. 61 (2013) 7816–7827.

[25] Y.H. Zhang, S. Xu, H.R. Fu, J. Lee, J. Su, K.C. Hwang, et al., Buckling in serpentine microstructures and applications in elastomer-supported ultra-stretchable electronics with high areal coverage, Soft Matter 9 (2013) 8062–8070.

[26] Y. Zhang, H. Fu, S. Xu, J.A. Fan, K.-C. Hwang, J. Jiang, et al., A hierarchical computational model for stretchable interconnects with fractal-inspired designs, J. Mech. Phys. Solids 72 (2014) 115–130.

[27] Y. Qi, J. Kim, T.D. Nguyen, B. Lisko, P.K. Purohit, M.C. McAlpine, Enhanced piezoelectricity and stretchability in energy harvesting devices fabricated from buckled PZT ribbons, Nano Lett. 11 (2011) 1331–1336.

[28] T. Ma, Y. Wang, R. Tang, H. Yu, H. Jiang, Pre-patterned ZnO nanoribbons on soft substrates for stretchable energy harvesting applications, J. Appl. Phys. 113 (2013).

[29] Y. Qi, T.D. Nguyen, P.K. Purohit, M.C. McAlpine, Stretchable piezoelectric nanoribbons for biocompatible energy harvesting, in: T. Someya (Ed.), Stretchable Electronics, Wiley-VCH Verlag GmbH & Co. KGaA, 2013.

[30] D. Brosteaux, F. Axisa, M. Gonzalez, J. Vanfleteren, Design and fabrication of elastic interconnections for stretchable electronic circuits, IEEE Electron Device Lett. 28 (2007) 552–554.

[31] U. Betz, M.K. Olsson, J. Marthy, M.F. Escola, F. Atamny, Thin films engineering of Indium Tin Oxide: large area flat panel displays application, Surf. Coat. Technol. 200 (2006) 5751–5759.

[32] H. Schmidt, H. Flugge, T. Winkler, T. Bulow, T. Riedl, W. Kowalsky, Efficient semitransparent inverted organic solar cells with Indium Tin Oxide top electrode, Appl. Phys. Lett. 94 (2009).

[33] Y. Leterrier, L. Medico, F. Demarco, J.A.E. Manson, U. Betz, M.F. Escola, et al., Mechanical integrity of transparent conductive oxide films for flexible polymer-based displays, Thin Solid Films 460 (2004) 156–166.

[34] C. Peng, Z. Jia, D. Bianculli, T. Li, J. Lou, In situ electro-mechanical experiments and mechanics modeling of tensile cracking in Indium Tin Oxide thin films on polyimide substrates, J. Appl. Phys. 109 (2011).

[35] C. Peng, Z. Jia, H. Neilson, T. Li, J. Lou, In situ electro-mechanical experiments and mechanics modeling of fracture in Indium Tin Oxide-based multilayer electrodes, Adv. Eng. Mater. 15 (2013) 250–256.
[36] S. Yang, B. Su, G. Bitar, N. Lu, Stretchability of Indium Tin Oxide (ITO) serpentine thin films supported by Kapton substrates, Int. J. Fract. 190 (2014) 99–110.
[37] P. Gutruf, C.M. Shah, S. Walia, H. Nili, A.S. Zoolfakar, C. Karnutsch, et al., Transparent functional oxide stretchable electronics: micro-tectonics enabled high strain electrodes, NPG Asia Mater. 5 (2013).
[38] J. George, C.S. Menon, Electrical and optical properties of electron beam evaporated ITO thin films, Surf. Coat. Technol. 132 (2000) 45–48.
[39] F.L. Wong, M.K. Fung, S.W. Tong, C.S. Lee, S.T. Lee, Flexible organic light-emitting device based on magnetron sputtered indium-tin-oxide on plastic substrate, Thin Solid Films 466 (2004) 225–230.
[40] Y.Y. Hsu, M. Gonzalez, F. Bossuyt, F. Axisa, J. Vanfleteren, I. De Wolf, The effects of encapsulation on deformation behavior and failure mechanisms of stretchable interconnects, Thin Solid Films 519 (2011) 2225–2234.
[41] Y.Y. Hsu, M. Gonzalez, F. Bossuyt, F. Axisa, J. Vanfleteren, I. De Wolf, The effect of pitch on deformation behavior and the stretching-induced failure of a polymer-encapsulated stretchable circuit, J. Micromech. Microeng. 20 (2010).
[42] T.W. Shield, K.S. Kim, R.T. Shield, The buckling of an elastic layer bonded to an elastic substrate in plane-strain, J. Appl. Mech.—Trans. ASME 61 (1994) 231–235.
[43] G. Gioia, M. Ortiz, Delamination of compressed thin films, Adv. Appl. Mech. 33 (1997) 119–192.
[44] J. Liang, R. Huang, H. Yin, J.C. Sturm, K.D. Hobart, Z. Suo, Relaxation of compressed elastic islands on a viscous layer, Acta Mater. 50 (2002) 2933–2944.
[45] H.X. Mei, R. Huang, J.Y. Chung, C.M. Stafford, H.H. Yu, Buckling modes of elastic thin films on elastic substrates, Appl. Phys. Lett. 90 (2007).
[46] D. Vella, J. Bico, A. Boudaoud, B. Roman, P.M. Reis, The macroscopic delamination of thin films from elastic substrates, Proc. Natl. Acad. Sci. USA 106 (2009) 10901–10906.
[47] S. Goyal, K. Srinivasan, G. Subbarayan, T. Siegmund, On instability-induced debond initiation in thin film systems, Eng. Fract. Mech. 77 (2010) 1298–1313.
[48] H.X. Mei, C.M. Landis, R. Huang, Concomitant wrinkling and buckle-delamination of elastic thin films on compliant substrates, Mech. Mater. 43 (2011) 627–642.
[49] H. Jiang, D. Khang, J. Song, Y. Sun, Y. Huang, J. Rogers, Finite deformation mechanics in buckled thin films on compliant supports, Proc. Natl. Acad. Sci. USA 104 (2007) 15607–15612.
[50] J. Song, H. Jiang, Z. Liu, D. Khang, Y. Huang, J. Rogers, et al., Buckling of a stiff thin film on a compliant substrate in large deformation, Internat. J. Solids Structures 45 (2008) 3107–3121.